

## Protein Engineering

# Chemoenzymatic Synthesis and Protein Engineering Enable Efficient, Scalable Production of Teleocidin Derivatives

Shuo Zheng<sup>+</sup>, Zixuan Yang<sup>+</sup>, Xiang Long, Xinying Ge, Zhiqin Zhang, Yinyin Feng, Yangyizhuo Li, Bo Gu, Yan Long, Xuanliang Yang, Rui Xu, and Heng Song\*

**Abstract:** Monoterpenoid indole alkaloids (MIAs), a class of bioactive natural products, are highly valued in drug development for their unique pharmacological activities. Teleocidins, known for activating protein kinase C (PKC), are particularly promising but challenging to synthesize due to their structural complexity. Traditional methods often rely on heavy metals and yield low amounts, while biosynthetic approaches face efficiency issues. Our study developed an efficient chemoenzymatic route to produce 13 teleocidin B compounds and derivatives at scale. To overcome enzymatic reaction bottlenecks, we engineered the critical enzyme TleB by fusing a reductase module to create a self-sufficient P450 system, boosting indolactam V production to 868.8 mg L<sup>-1</sup>. Additionally, we established a dual-cell factory co-expressing engineered hMAT2A-TleD and TleB/TleC enzymes, enabling the first fully enzymatic synthesis of teleocidin B isomers with a total yield of 714.7 mg L<sup>-1</sup>. Chemical modifications further expanded the library with five novel indolactam V and two teleocidin A1 derivatives. Fermentation confirmed the recombinant *Escherichia coli* system's scalability, producing 430 mg indolactam V, 170 mg teleocidin A1, and 300 mg teleocidin B isomers. This work not only establishes a sustainable platform for teleocidin synthesis but also addresses efficiency and scalability challenges in complex natural product synthesis, paving the way for practical applications of bioactive compounds.

## Introduction

Monoterpene indole alkaloids (MIAs) represent a prominent frontier in natural product medicinal chemistry, attracting significant attention due to their remarkable structural diversity, diverse therapeutic applications, and high translational potential.<sup>[1–5]</sup> To date, over 3000 distinct MIA structures have been elucidated, with notable examples including clinically established drugs like vinblastine, camptothecin, and quinine, alongside pharmacologically relevant compounds such as strychnine and rosantinn.<sup>[1–4]</sup> Of particular interest within this family are the teleocidins and their biosynthetic precursors (Scheme 1a), which exhibit unique structural architectures

among MIAs and possess exceptional biological significance as potent activators of protein kinase C (PKC).<sup>[6,7]</sup> This distinctive pharmacological property positions teleocidins as valuable tools for dissecting cellular signaling pathways implicated in human pathologies, particularly their promising applications in oncology as potential anticancer therapeutics.<sup>[8–10]</sup>

The limited natural abundance of teleocidins and incomplete genetic understanding of their producing *Streptomyces* strains present major bottlenecks to scalable production.<sup>[11,12]</sup> These challenges are compounded by the paucity of genetic tools for metabolic engineering and difficulties in scaling fermentation processes. While chemical synthesis approaches—including electrochemical methods, metal-catalyzed reactions, and ligand-assisted strategies—have successfully produced teleocidins,<sup>[13–18]</sup> they remain hindered by lengthy synthetic routes, reliance on toxic heavy metals, and poor overall yields.<sup>[13]</sup> Recent cell-free biosynthesis efforts reported teleocidin B4 production with the addition of exogenous redox partners, though yields remain unverified.<sup>[19]</sup> To overcome these limitations, particularly for synthesizing complex teleocidin analogs, leveraging their native biosynthetic enzymes appears promising. These enzymes inherently control stereochemistry and regioselectivity without protective group chemistry, complementing traditional synthetic methods. Their amenability to protein engineering enables the development of optimized biocatalysts with enhanced or novel activities. Integrating enzymatic transformations into synthetic workflows thus offers innovative, streamlined pathways for efficient teleocidin production, potentially overcoming current scalability and yield challenges.


[\*] S. Zheng<sup>+</sup>, Z. Yang<sup>+</sup>, X. Ge, Z. Zhang, Y. Feng, Y. Li, B. Gu, Y. Long, X. Yang, Prof. H. Song  
 College of Chemistry and Molecular Sciences, Wuhan University,  
 Wuhan, Hubei Province, P.R. China  
 E-mail: [hengsong@whu.edu.cn](mailto:hengsong@whu.edu.cn)

Prof. H. Song  
 Wuhan University Shenzhen Research Institute, Wuhan University,  
 Shenzhen, Guangdong Province, P.R. China

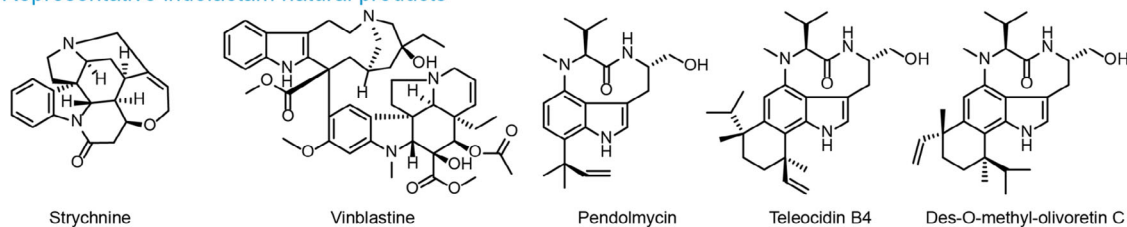
X. Long, R. Xu  
 Hubei Vocational College of Bio-Technology, Wuhan, Hubei  
 Province, P.R. China

X. Long  
 School of Cyber Space Security, Huazhong University of Science and  
 Technology, Wuhan, Hubei Province, P.R. China

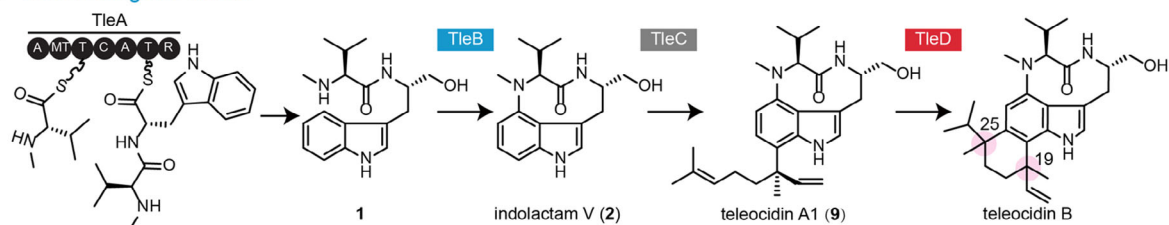
[<sup>+</sup>] Both authors contributed equally to this work.

 Additional supporting information can be found online in the  
 Supporting Information section

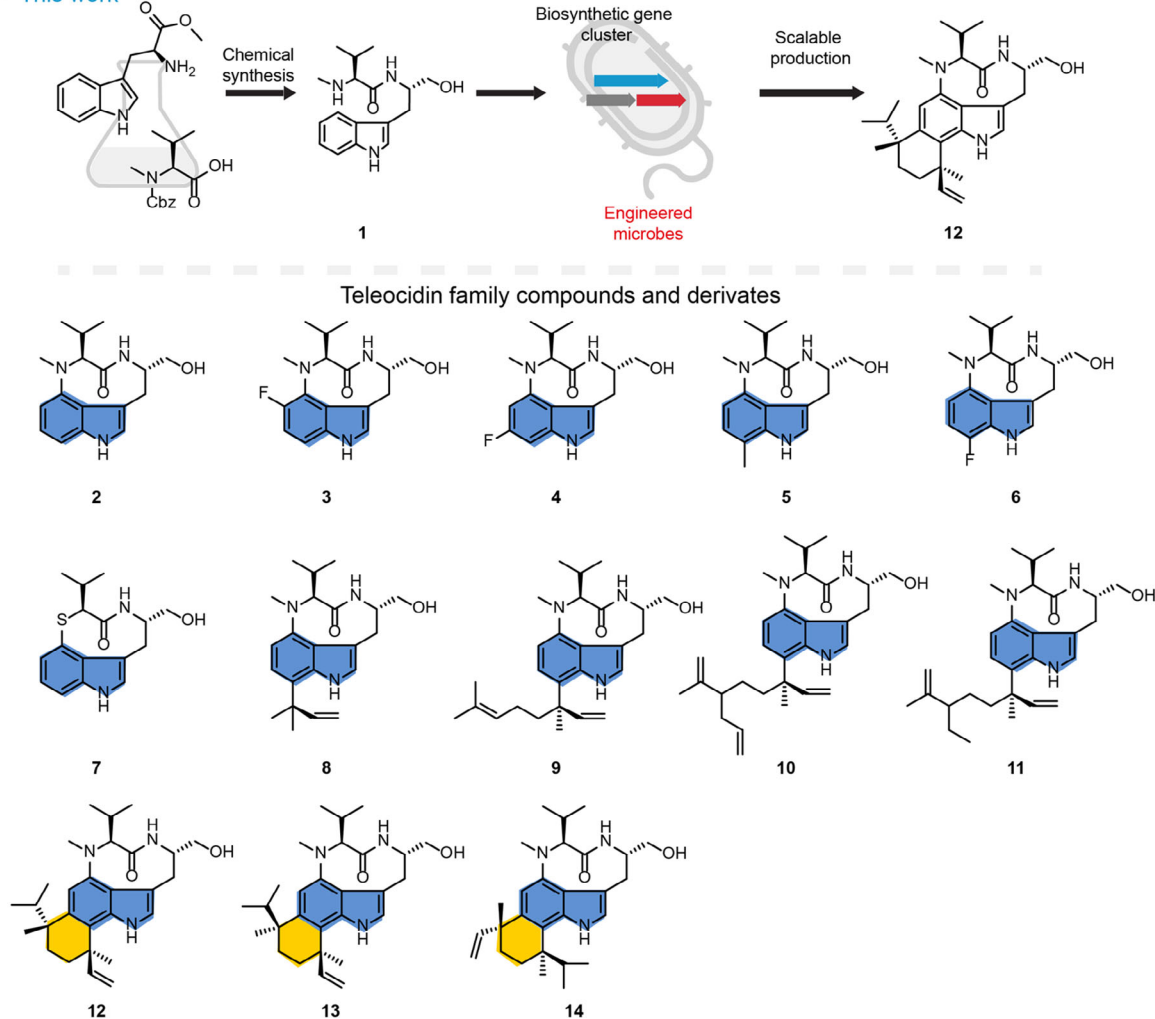
## a Representative indolactam natural products



## b Teleocidin gene cluster



## c This work



**Scheme 1.** Merging biological and chemical strategies to expand the scope of teleocidin family production. a) Structure of representative monoterpene indole alkaloids. b) The complete biosynthetic pathway of teleocidins. c) Scalable chemoenzymatic platform enabling divergent synthesis of 13 structurally diverse teleocidin B congeners and derivatives.

The complete biosynthetic pathway of teleocidins and their derivatives (depicted in Scheme 1b) has been elucidated. This intricate process commences with the enzyme-catalyzed formation of *N*-methyl-L-valyl-L-tryptophanol (NMVT, **1**) from tryptophan by TleA.<sup>[20]</sup> Subsequently, a multi-enzyme complex comprising TleB, CamA, and CamB mediates the conversion of NMVT (**1**) to the key intermediate indolactam V (**2**) through a series of coordinated reactions.<sup>[20–22]</sup> Of particular interest is the challenging cyclization step that constructs the strained nine-membered ring intermediate (**2**), a transformation that inherently defies conventional synthetic logic due to significant ring strain and entropic penalties as predicted by Baldwin's Rules. Downstream, TleC facilitates the conversion of indolactam V (**2**) to teleocidin A1 (**9**),<sup>[23]</sup> which is subsequently transformed into teleocidin B (**12–14**) by TleD (Scheme 1).<sup>[24]</sup> However, these naturally evolved enzymes, originally optimized for secondary metabolite production, exhibit limitations in catalytic efficiency, operational practicality, and scalability when applied to synthetic chemistry platforms. To address these deficiencies, systematic enzyme engineering strategies coupled with reaction parameter optimization appear essential for enhancing enzymatic performance to support synthetic endeavors. Furthermore, the development of engineered biocatalysts through protein redesign could enable access to novel “new-to-nature” analogs of indolactam V and teleocidins. Although heterologous expression systems using microbial hosts like *E. coli*<sup>[25–31]</sup> hold promise for efficient biosynthesis, no successful reports exist demonstrating teleocidin production via whole-cell biocatalysis. Therefore, achieving high-titer production may necessitate hybrid chemical-enzymatic strategies that combine the strengths of both synthetic approaches, offering a promising pathway toward efficient and scalable manufacturing.

In this study, we established a streamlined chemoenzymatic strategy for high-yield production of teleocidin family compounds. Commencing with commercially available L-tryptophan methyl ester and Cbz-protected *N*-methyl-L-valine, we synthesized NMVT (**1**) via amide coupling (Figures 1a and S5). This efficient organic synthesis step established the foundation for subsequent enzymatic transformations. Through rational chimeric protein engineering of TleB, we constructed a synthetic one-component self-sufficient P450 enzyme that dramatically enhanced indolactam V (**2**) biosynthesis, resulting in a remarkable 14-fold yield improvement. Subsequent optimization of TleC/MpnD expression enabled teleocidin A1 (**9**) and pendolmycin (**8**) biosynthesis using geranyl pyrophosphate (GPP)/dimethylallyl pyrophosphate (DMAPP) precursors. A dual-cell system co-expressing hMAT2A-TleD fusion with TleC/TleB-CamAB facilitated cytosolic teleocidin B production (**12–14**). Beyond natural analogs, this platform supported chemoenzymatic synthesis of five indolactam V derivatives and two teleocidin A1 variants, showcasing structural diversification capabilities. Notably, fermentation-derived biocatalysts yielded 430 mg indolactam V (**2**), 170 mg teleocidin A1 (**9**), and 300 mg teleocidins (**12**, **13**, and **14**), demonstrating practical scalability. This modular, yield-optimized platform demonstrates innovative strategies for natural product drug development and complex

biosynthesis, offering exceptional adaptability and efficiency that underscore promising pathways for scalable production of high-value bioactive compounds.

## Results and Discussion

### Engineering Artificial Self-Sufficient P450 TleB for the Synthesis of Indolactam V and Its Derivatives

Our chemo-biosynthetic analysis of teleocidin B family compounds (Figure 1a) commenced with the commercially available L-(–)-tryptophan methyl ester hydrochloride and Cbz-protected *N*-methyl-L-valine, which were condensed via amide bonds to yield NMVT (**1**) as the substrate for subsequent TleB catalysis. This step served as a surrogate for the enzyme TleA, which exhibits suboptimal expression and activity in heterologous hosts. For intermediates that are more accessible, organic synthesis offers a rapid and cost-effective means of production. To expedite NMVT (**1**) synthesis, we utilized economically viable and accessible starting materials, facilitating rapid production through a three-step synthesis process (Figure S5). Within it, L-(–)-tryptophan methyl ester hydrochloride was reduced using NaBH<sub>4</sub> to yield tryptophol. Under standard amide coupling conditions, tryptophol was linked via an amide bond to Cbz-protected *N*-methyl-L-valine. Following deprotection of the Cbz group, the NMVT (**1**) substrate was obtained. The intramolecular C–N coupling of NMVT (**1**), catalyzed by the P450 enzyme HinD and its homolog TleB, in conjunction with redox chaperone proteins CamA and CamB, resulted in the formation of a nine-membered indolactam backbone.<sup>[20]</sup>

Traditional enzyme discovery efforts in secondary metabolite biosynthesis often do not prioritize reaction efficiency, practicality, and scalability—essential criteria for synthetic biology applications. A pivotal step in teleocidin B biosynthesis is the enzymatic formation of a nine-membered ring, catalyzed by the P450 enzymes HinD or TleB. In this study, TleB was prioritized for initial strain engineering due to its higher expression levels compared to HinD (Figure S17). Notably, most P450 enzymes function within multiprotein complexes, relying on redox partners—such as FAD/Fe<sub>2</sub>S<sub>2</sub> clusters in Class I systems or FAD/FMN cofactors in Class II systems—to shuttle electrons from NADH/NADPH to the heme active site. The native redox machinery for TleB remains undefined, necessitating the use of surrogate partners for in vitro reconstitution. Previously, ferredoxin (CamA) and ferredoxin-NADP<sup>+</sup>reductase (CamB) were employed to restore TleB activity.<sup>[20,32]</sup> To assess whether soluble CamA and CamB domains could independently support TleB catalysis, we engineered an *E. coli* BL21-DE3 strain (P1 variant) co-expressing TleB, CamA, and CamB from pACYC plasmids and SDS-PAGE confirmed successful protein expression (Figure S17). Whole-cell biotransformations were conducted at 30 °C in Tris buffer (pH 8.5) using 150 mg wet cells per mL reaction mixture and 3 mM NMVT (**1**). The initial three-component system yielded modest indolactam V titers (**2**, 61.3 mg L<sup>–1</sup>), underscoring the need for optimization. Inspired by the RhFRed fusion

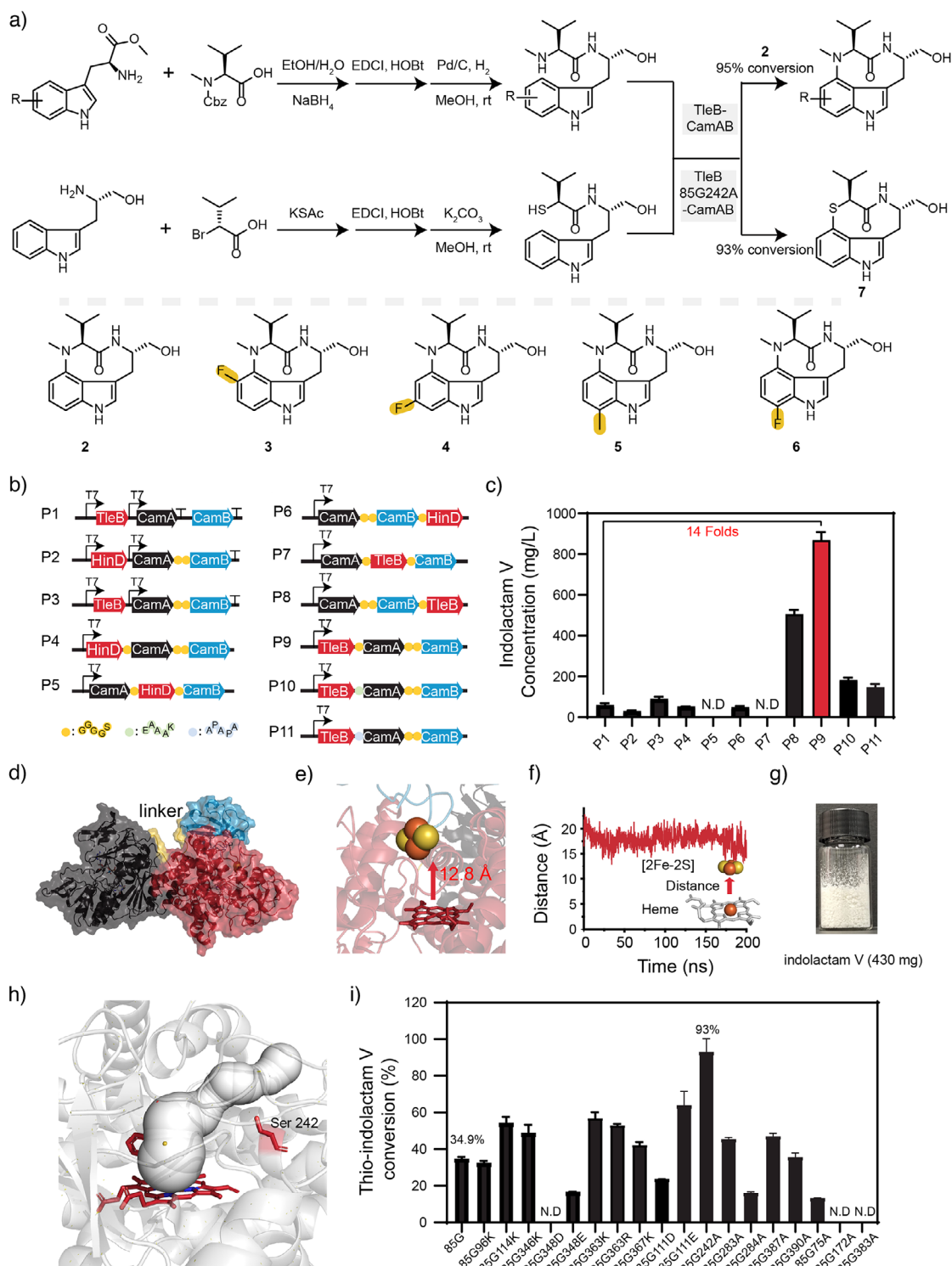


**Figure 1.** Engineering artificial self-sufficient P450 TleB for indolactam V and its derivative production. a) Chemoenzymatic synthesis route of indolactam V and its derivatives. It commenced with the commercially available L-(−)-tryptophan methyl ester hydrochloride and Cbz-protected N-methyl-L-valine or (R)-2-bromo-3-methylbutanoic acid and tryptophan. The substitute of indolactam V is marked in yellow. b) Engineered TleB for indolactam V and its derivatives production in *E. coli*. The system includes the three-component plasmid P1, the two-component plasmids P2 and P3, and eight self-sufficient P450 TleB plasmids P4-P11. T7: T7 promoter. G: Gly, S: Ser. E: Glu, A: Ala, K: Lys. c) Production titers of indolactam V by *E. coli* expressing 11 engineered TleB. Data are of three biological replicates. d) Predicted structure of TleB-GGGGS-CamAB via AlphaFold2. TleB, CamA, and CamB are marked in red, black, and blue, respectively, while linker between proteins is marked in yellow. e) Predicted TleB-GGGGS-CamAB protein structure of heme-Fe and [2Fe-2S] region. f) Distance evolutions between the [2Fe-2S] cluster and the heme-Fe during the MD simulations. g) Purified indolactam V product obtained from P9 fermentation. h) Crystal structure of TleB (pdb: 8jrl). The substrate channel predicted by the caver appeared white. i) Effects of salt bridge and substrate channel mutant on conversion of thio-indolactam V. Conversion was determined by HPLC.



scaffold,<sup>[33]</sup> we engineered CamA-CamB fusion proteins to recapitulate native redox synergy, generating the P3 variant. For comparative analysis, we also produced fusion variants (P2) with HinD. Biotransformation assays demonstrated a 1.5-fold enhancement in catalytic efficiency for P3-containing cells, achieving 92.2 mg L<sup>-1</sup> indolactam V (**2**) compared to 31.1 mg L<sup>-1</sup> for P2-containing cells (Figure 1c). This significant improvement validates P3 as a promising candidate for downstream process development, warranting further structural and mechanistic characterization to elucidate its enhanced performance.

Previous studies have established that fusing P450 enzymes with their redox partners enhances electron transfer efficiency by reducing spatial separation between components.<sup>[33–35]</sup> However, such fusion strategies often compromise native protein functionality and catalytic efficiency, as previously documented.<sup>[36,37]</sup> To address this limitation, we systematically optimized fusion architectures between TleB/HinD and CamA/CamB to maximize product titer (Figure 1b). This single-component, self-sufficient P450 system—driven by NADH—reproduced the full physiological reaction spectrum of natively supported TleB systems.<sup>[38–41]</sup> Initial designs positioned HinD and TleB at the N-terminal (P4 and P9), central (P5 and P7), or C-terminal (P6 and P8) regions of three-component fusion proteins (Figure 1b). Following construction and co-expression of six fusion variants, complete loss of enzymatic activity in the CamA-HinD(TleB)-CamB configuration suggested that P450 positioning critically influences fusion protein functionality. Notably, the TleB-CamA-CamB fusion (P9) achieved an indolactam V (**2**) titer of 868.8 mg L<sup>-1</sup>, representing a 14-fold improvement over the non-fused system (Figure 1c). We also replaced GGGGS with rigid linker (EAAAK or APAPA) to increase indolactam V (**2**) titer but observed no improvement (Figure 1c).

To systematically evaluate redox partner compatibility, we replaced the CamAB system with heterologous Fdx/Fdr chaperones derived from spinach and *Chlorella*, generating four fusion variants (P16–P19) (Figure S22). Among these constructs, the TleB-Fdx(spinnach)-Fdr chimera exhibited the highest catalytic activity, producing indolactam V (**2**) at 496.7 mg L<sup>-1</sup>—representing a 33% enhancement compared to the non-fusion control. Notably, this titer remained 1.7-fold lower than the optimized TleB-GGGGS-CamAB fusion, highlighting that both redox partner identity and spatial orientation critically influence catalytic outcomes. Even when domain positioning is optimized, the intrinsic electron transfer capabilities of different chaperone systems emerge as the determining factor in overall catalytic efficiency.

Since structural–functional analysis can aid in understanding the interactions between P450 enzymes and their redox partners, AlphaFold2-Multimer was used to predict the crystal structures of P1–P11 (Figure S13). Subsequently, 11 complex structures were generated. The results showed that the [2Fe-2S]-to-heme distance exceeded 20 Å in P5 and P7, which was not conducive to efficient electron transfer for P450 enzyme catalysis and consistent with the experimental results (Figure S13). The remaining fusion proteins exhibited shorter [2Fe-

2S]-to-heme distances, ranging from 14.7 to 17.5 Å, potentially enabling tighter electron transfer pathways.

However, static structural simulations may not sufficiently explain why the P9 fusion protein exhibits the highest activity enhancement. Therefore, we performed molecular dynamics (MD) simulations on the highest-activity P9 fusion protein using Gromacs 2019. Over 200 ns at ambient conditions, the shortest [2Fe-2S]-to-heme distance stabilized at 12.8 Å (Figure 1e,f), below the biological electron transfer threshold (14–15 Å).<sup>[38]</sup> This proximity suggests direct, efficient electron transfer between clusters. Kinetic analyses revealed a 40-fold increase in  $k_{\text{cat}}$  ( $61.1 \pm 3.2 \text{ min}^{-1}$  versus  $1.51 \pm 0.05 \text{ min}^{-1}$ ) and a 6.3-fold improvement in  $k_{\text{cat}}/K_{\text{m}}$  ( $5.01$  versus  $0.80 \text{ s}^{-1} \text{ mM}^{-1}$ ) for the fusion construct (Figures S15 and S16). Collectively, these findings provide a mechanistic rationale for the observed enhancements in TleB catalytic efficiency.

To maximize indolactam V (**2**) production, we systematically investigated critical reaction parameters. Optimal conditions were identified as pH 8.5 and OD<sub>600</sub> 90, yielding a peak titer of 868.8 mg L<sup>-1</sup> (Figure S21). To evaluate the scalability of our engineered *E. coli* system, P9 cells were cultivated in a 20-L bioreactor for NMVT-to-indolactam V bioconversion. A portion of harvested biomass facilitated the production of 430 mg indolactam V (Figure 1g), confirming robust scalability at pilot scale. Furthermore, structural diversification was demonstrated by synthesizing four NMVT analogs from L-(–)-tryptophan methyl ester derivatives and Cbz-protected N-methyl-L-valine (Figures 1a and S5). These analogs were successfully converted into indolactam V derivatives using P9 whole-cell biocatalysis, highlighting the system's versatility for generating chemically diverse derivatives.

As a structural analog of indolactam V, thio-indolactam V can selectively bind to Ca<sup>2+</sup>-independent PKC isozymes due to its SOFA-restricted conformation; thus, the molecular targets of thio-indolactam V are likely different from those of TWIST-restricted analog of indolactam V.<sup>[21]</sup> Considering its special potential as an anticancer drug, we tried to acquire thio-indolactam V using the established chemoenzymatic platform. To rapidly synthesize thio-indolactam V, a chemoenzymatic route was developed. Initially, the non-racemic substrate was prepared chemically: (R)-2-bromo-3-methylbutanoic acid reacted with potassium thioacetate, stereospecifically yielding (S)-2-(acetylthio)-3-methylbutanoic acid. Subsequently, this product underwent EDCI/HOBt-mediated condensation with tryptophan to form the amide bond. Following deacetylation, the desired 13-sulfhydryl (13-SH)-substituted NMVT was obtained.

TleB L85G-CYP116B46 was a reported protein for only producing thio-indolactam V.<sup>[42]</sup> Subsequently, P9 L85G was used to catalyze this substrate, which produced the target product exclusively but with a low initial conversion rate (34.9%). To enhance catalytic efficiency, site-directed mutagenesis was performed by rationally redesigning salt bridges and substrate channels. We first screened native salt bridge pairs on the protein surface (e.g., R367-D120 and R114-D150). To construct novel salt bridge interactions, we implemented two strategies: (1) replacing residues at these positions with amino acids of the same charge polarity and (2)

mutating neighboring residues. Among these modifications, the L85GS363K double mutant successfully increased the substrate conversion rate from 34.9% to 56.7% (Figure 1i). Subsequently, substrate binding channels were predicted using Caver software, followed by alanine scanning mutagenesis targeting key residues surrounding these channels (including S242, K383, S283, H284, etc.). The engineered enzyme variant P9-85G242A significantly improved reaction performance, successfully increasing the conversion to 93% (Figure 1i). The reactions were scaled, and derivatives **7** were purified and validated by  $^1\text{H}$  NMR (Figure S54).

### Enzymatic Synthesis of Teleocidin A1 and Pendolmycin

Having established the engineered TleB-GGGGS-CamAB fusion enzyme, we next targeted the biosynthesis of teleocidin A1 (**9**) and pendolmycin (**8**). To achieve this, we selected two isoprenoid transferases—TleC from *Streptomyces* and MpnD from *thermotolerant marine bacteria*<sup>[23]</sup>—to catalyze the C-7 reverse isoprenoylation of indolactam V (**2**) using geranyl pyrophosphate (GPP) or dimethylallyl pyrophosphate (DMAPP) as donors (Figure 2a). The synthetic module was designed by co-expressing the TleB-GGGGS-CamAB fusion with either TleC or MpnD in *E. coli*, under oxygen-rich conditions and in the presence of GPP/DMAPP.

For validation, we constructed *E. coli* strains co-expressing TleC/MpnD with the fusion enzyme (Figure 2b). Initial whole-cell biotransformation assays demonstrated functional activity, producing teleocidin A1 (**9**, 27.4 mg L<sup>-1</sup>) and pendolmycin (**8**, 39.2 mg L<sup>-1</sup>) from indolactam V (Figure S31). To enhance productivity, we systematically optimized enzymatic parameters (Figure S31). Notably, after optimization, teleocidin A1 (**9**) titers increased 31-fold to 868.7 mg L<sup>-1</sup> (3 mM substrate), while pendolmycin (**8**) production improved 6-fold to 246.1 mg L<sup>-1</sup> (1 mM substrate) (Figure 2c,d).

### Enzymatic Synthesis of Teleocidin A1 Derivatives

Next, we aimed to construct a biosynthesis module for teleocidin B and teleocidin A1 derivatives (Figure 3a). Human methionine adenosine transferases hMAT2A and TleD were selected based on their capacity to metabolize methionine and teleocidin A1 (**9**) into teleocidin B (**12–14**). In this pathway, hMAT2A first converts methionine and ATP into S-adenosylmethionine (SAM), which TleD subsequently utilizes to install the methyl group into teleocidin A1 (Figure 3a). A critical challenge was intracellular competition among SAM-dependent enzymes, which could compromise TleD efficiency. To mitigate this, we sequentially integrated hMAT2A and TleD into *E. coli*, enabling efficient in situ SAM generation. This strain achieved a high teleocidin B titer of 1980.7 mg L<sup>-1</sup> using teleocidin A1 (**9**) as the substrate (Figure 3a,b).

Building on this success, we sought to generate novel teleocidin A1 derivatives leveraging hMAT2A's ability to produce 29 non-natural SAM analogs.<sup>[43]</sup> To ensure sufficient teleocidin A1 supply, we scaled TleC fermentation

to 2 L, yielding 170 mg of purified teleocidin A1 (**9**). A chemoenzymatic cascade was then established using hMAT2A and TleD to access new-to-nature derivatives (Figure 3e). We synthesized three halogenated methionine derivatives in a one-step reaction via Na-mediated reductive alkylation of L,L-homocystine with corresponding iodoalkanes in liquid NH<sub>3</sub> at -78 °C (Figure S3). Meanwhile, L-methionine was subjected to esterification followed by N-Boc protection to afford N-Boc-L-methionine methyl ester. Subsequent alkylation with haloalkanes yielded protected analogs. Deprotection and saponification then furnished the allyl- and propargyl-functionalized methionine derivatives (Figure S4). hMAT2A efficiently converts five synthesized methionine derivatives and commercially available ethionine into corresponding SAM derivatives, excluding difluoroethyl- and trifluoromethyl-methionine derivatives. However, TleD exhibits significantly lower catalytic activity toward most derivatives, with allyl-methionine being the sole exception. To engineer functionally enhanced mutants, we employed a structurally conservative substitution strategy, selecting replacement residues with spatial/functional similarity to native residues. However, H37R, Y21F, V36A, G85S, and A136T failed to improve activity, with H37R abolishing catalysis entirely. Subsequently, through topological mapping of the SAM-binding pocket, we rationally targeted three residues proximal to key SAM moieties for alanine scanning: G87 overlying the methionine group, Q112 adjacent to the sulfonium sulfur, and V108 positioned above the adenine ring. TleD Q112A was identified as a beneficial mutant, significantly enhancing conversion rates for derivative **10**. Steric analysis suggested the allyl group's conformation in the active site may hinder 1,2-H shifts, favoring  $\beta$ -H elimination to form compound **10** (Figure 3e). Based on the relevant literature,<sup>[44]</sup> we employed the distance between the C25 atom of the substrate teleocidin A1 and the sulfur-attached carbon atom in the SAM molecule as an indicator to assess the reaction feasibility. Molecular dynamics results revealed that the distance between the carbon atom directly bonded to sulfur in the allyl group and C25 of teleocidin A1 fluctuated between 3.5 and 4.5 Å, suggesting a potential structural basis for enzymatic catalysis (Figure 3d). Further mutation (Q112Y) expanded substrate scope, enabling synthesis of compound **11**. Despite optimization challenges, the reactions were scaled, and derivatives **10/11** were purified and validated by  $^1\text{H}/^{13}\text{C}$  NMR (Figures S62 and S63).

### Chemoenzymatic Synthesis of Teleocidin B

Following validation of the three core enzymatic modules, we engineered a heterologous biosynthetic pathway for teleocidin B production in *E. coli*, commencing from NMVT (Figure 4a). The initial dual-plasmid system was constructed by cloning TleB-CamAB and TleC into pACYCDuet-1, while hMAT2A and TleD were inserted into a secondary pCDFDuet-1 vector (Figure 4b). Co-transformation of these plasmids into BL21(DE3) cells yielded strain M1A, with SDS-PAGE analysis confirming expression of all recombinant enzymes (Figure S37). Functional validation revealed success-

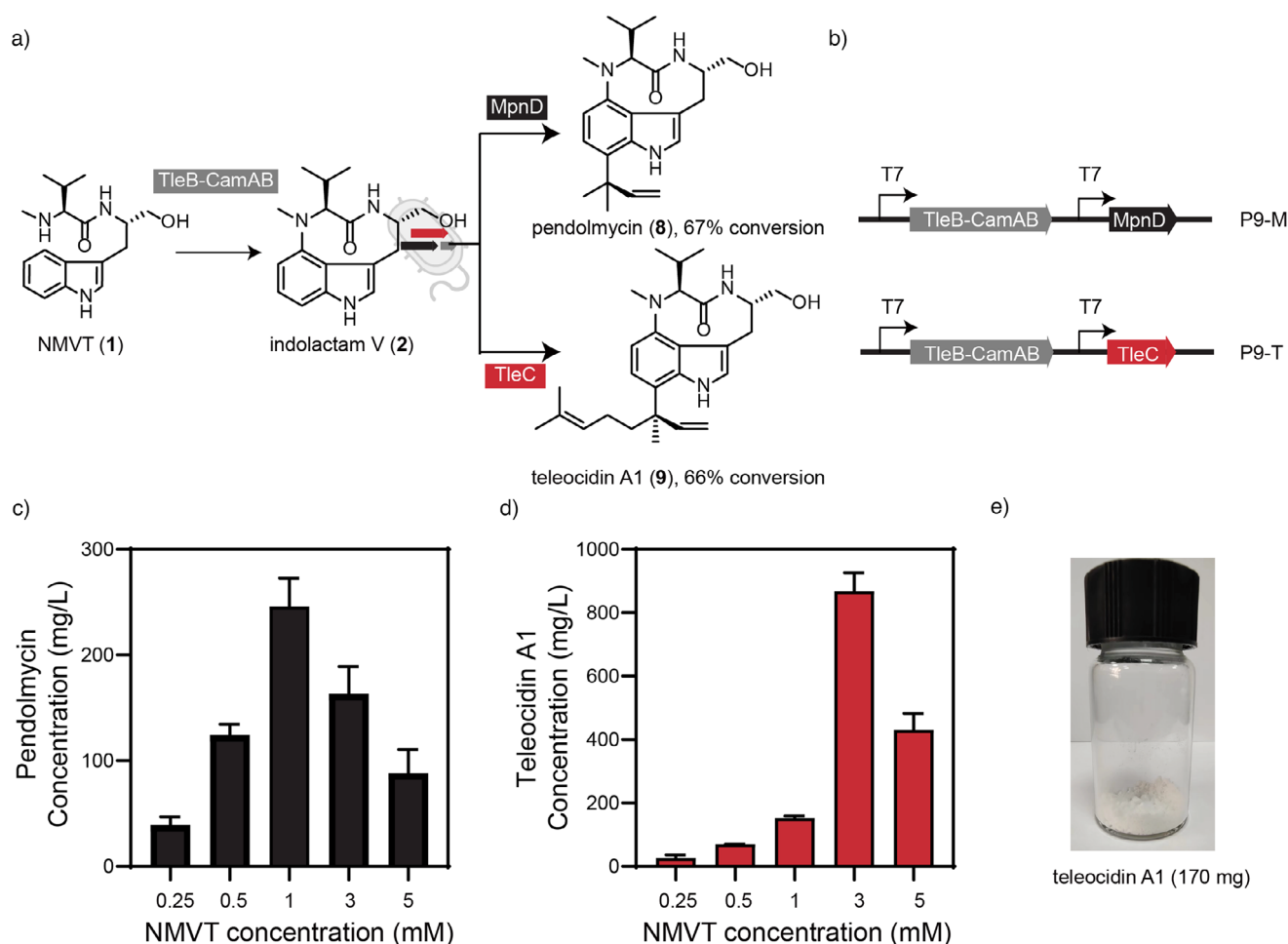


**Figure 2.** Biosynthesis of teleocidin A1 and pendolmycin. a) Schematic diagram of the teleocidin A1 and pendolmycin production. The system was designed by co-expressing the TleB-GGGGS-CamAB fusion protein with either TleC or MpnD in *E. coli*, in the presence of GPP/DMAPP. GPP, geranylpyrophosphate; DMAPP, dimethylallyl diphosphate. b) Engineered pathway for teleocidin A1 or pendolmycin production in *E. coli*. The system includes one plasmid with antibiotic markers, which encode for TleB-GGGGS-CamAB fusion protein and TleC or MpnD protein. T7: T7 promoter. c) Exploration for the catalytic limit of *E. coli* expressing TleB-GGGGS-CamAB fusion protein and MpnD protein. Data are of three biological replicates. d) Exploration for the catalytic limit of *E. coli* expressing TleB-GGGGS-CamAB fusion protein and TleC protein. Data are of three biological replicates. e) Purified teleocidin A1 product obtained from TleC fermentation.

ful one-pot conversion of NMVT (1) to teleocidin B (12–14) in M1A cultures, as evidenced by HPLC detection and product isolation (Figure 4c).

To enhance teleocidin B titers, we implemented a protein engineering strategy by creating hMAT2A-TleD fusion constructs. Linker optimization emerged as critical, with GS-rich flexible linkers (GS, GGGGS, GGGSGGGGS) and rigid linker (EAAAK, APAPA) evaluated for their impact on catalytic efficiency. Strain M1C, harboring the GGGGS linker, demonstrated superior performance with a 59.2 mg L<sup>-1</sup> yield improvement (Figure 4c).

Subsequent optimization efforts focused on resolving expression imbalances. SDS-PAGE profiling of M1C lysates revealed disproportionate accumulation of hMAT2A-TleD versus TleB-CamAB (Figure S39), likely due to higher copy number of the pCDFDuet-1 vector. To address this, we re-engineered the pathway by relocating TleB-CamAB and TleC to a high-copy pRSFDuet-1 vector, generating strain M2C (Figure 4b). However, this strategy

did not result in elevated expression of the TleB-GGGGS-CamAB protein, as confirmed through SDS-PAGE analysis of M1C and M2C (Figure S39). Despite the increased plasmid copy number, soluble protein yields remained comparable to the original expression system. This observation suggests that expression limitations may arise from translational rather than transcriptional constraints for this particular fusion protein. Consequently, M2A-M2F strains showed no yield improvement (Figure 4c).

Recognizing the limitations of single-cell co-expression, we adopted a bipartite cellular production strategy. Indolactam V (2) was first biosynthesized in *E. coli* expressing TleB-CamAB, followed by its conversion to teleocidin B (12–14) in a second strain harboring TleC and optimized hMAT2A-GGGGS-TleD (Figure 4a). This compartmentalized approach enabled independent enzyme regulation and reduced metabolic competition. For implementation, we generated strain M2 containing TleC and hMAT2A-GGGGS-TleD. The teleocidin B titer in dual-cell catalysis was limited to

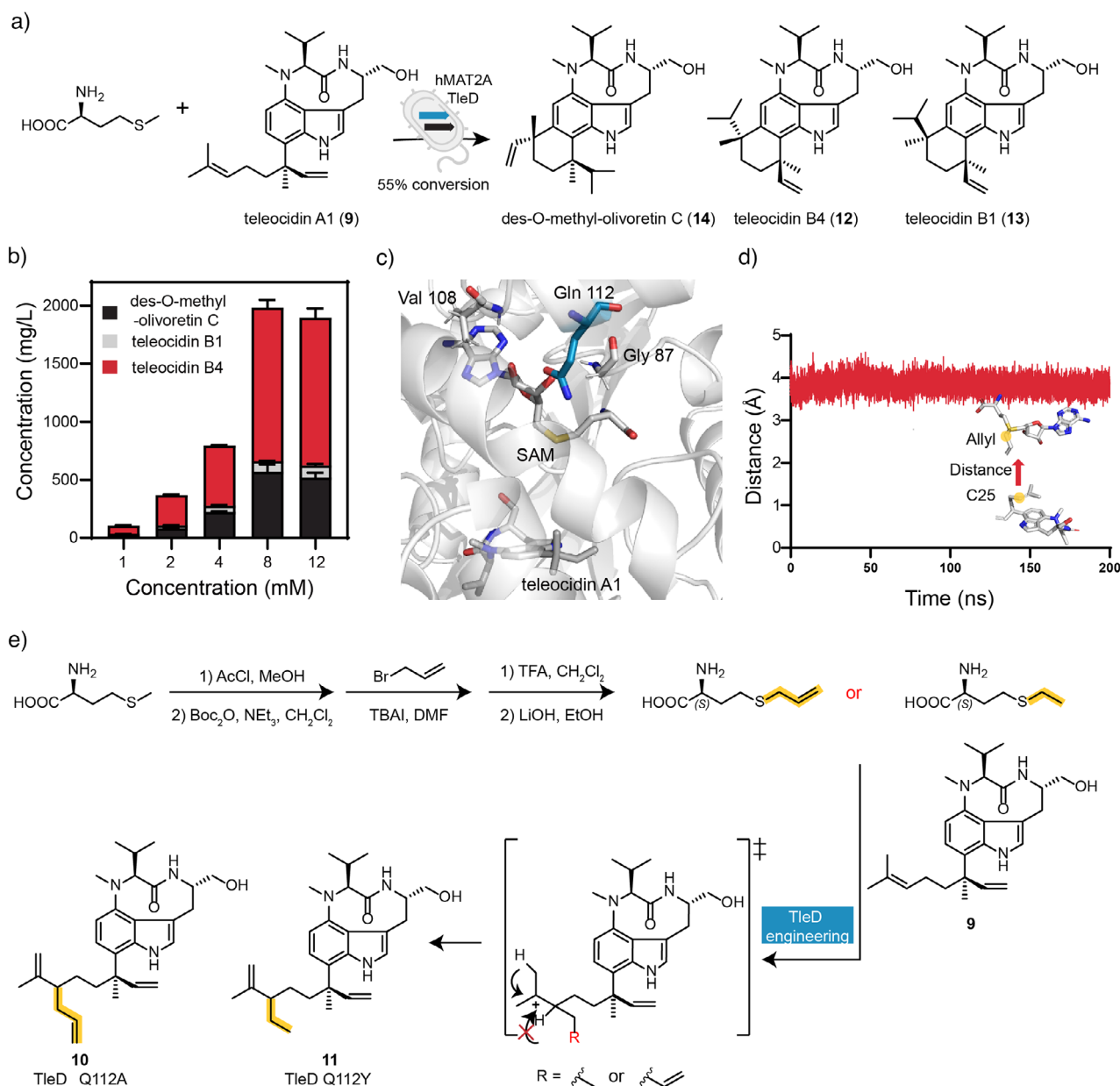


**Figure 3.** TleD engineering for production of teleocidin B and teleocidin A1 derivatives. a) Schematic diagram of the teleocidin B production. The system was designed by co-expressing the hMAT2A protein with TleD protein in *E. coli* in the presence of methionine. b) Exploration for the catalytic limit of *E. coli* expressing hMAT2A protein and TleD protein. Data are of three biological replicates. c) Crystal structure of TleD (pdb: 5GM2). The protein structure contains teleocidin A1 substrate and SAM cofactors. d) Distance between the carbon atom directly bonded to sulfur in the allyl group and C25 of teleocidin A1. e) Chemoenzymatic synthesis route of teleocidin A1 derivatives. It commenced with the commercially available L,L-homocysteine with corresponding halogenated alkanes.

87 mg L<sup>-1</sup>, potentially due to cross-cell metabolic interference or substrate transport limitations. To address the challenges of cross-cellular metabolic interference and substrate transport limitations, we implemented two complementary strategies to optimize the bioprocess: (1) incorporation of 1% *n*-butanol as a membrane-permeabilizing agent and (2) utilization of polyvinylpyrrolidone (PVP40) as a solubility-enhancing additive. Notably, the PVP40 formulation proved particularly effective, achieving a statistically significant 45% enhancement in teleocidin B production yield through its dual mechanisms of substrate solubilization and product sta-

bilization. These findings suggest that strategic modulation of membrane permeability and microenvironmental conditions can effectively mitigate transport bottlenecks in heterologous enzyme systems. Additionally, we introduced three tryptophan transporters into P9 cells in an attempt to enhance production; however, the production yield exhibited a marked decline (Figure S42). To further increase teleocidin B titer, we implemented a sequential reaction setup (Figure 4d), utilizing P9 cell supernatants and its cell precipitation lysate as substrates for M2 biocatalysis. This workflow achieved a breakthrough titer of 714.7 mg L<sup>-1</sup> teleocidin B (Figure 4e),



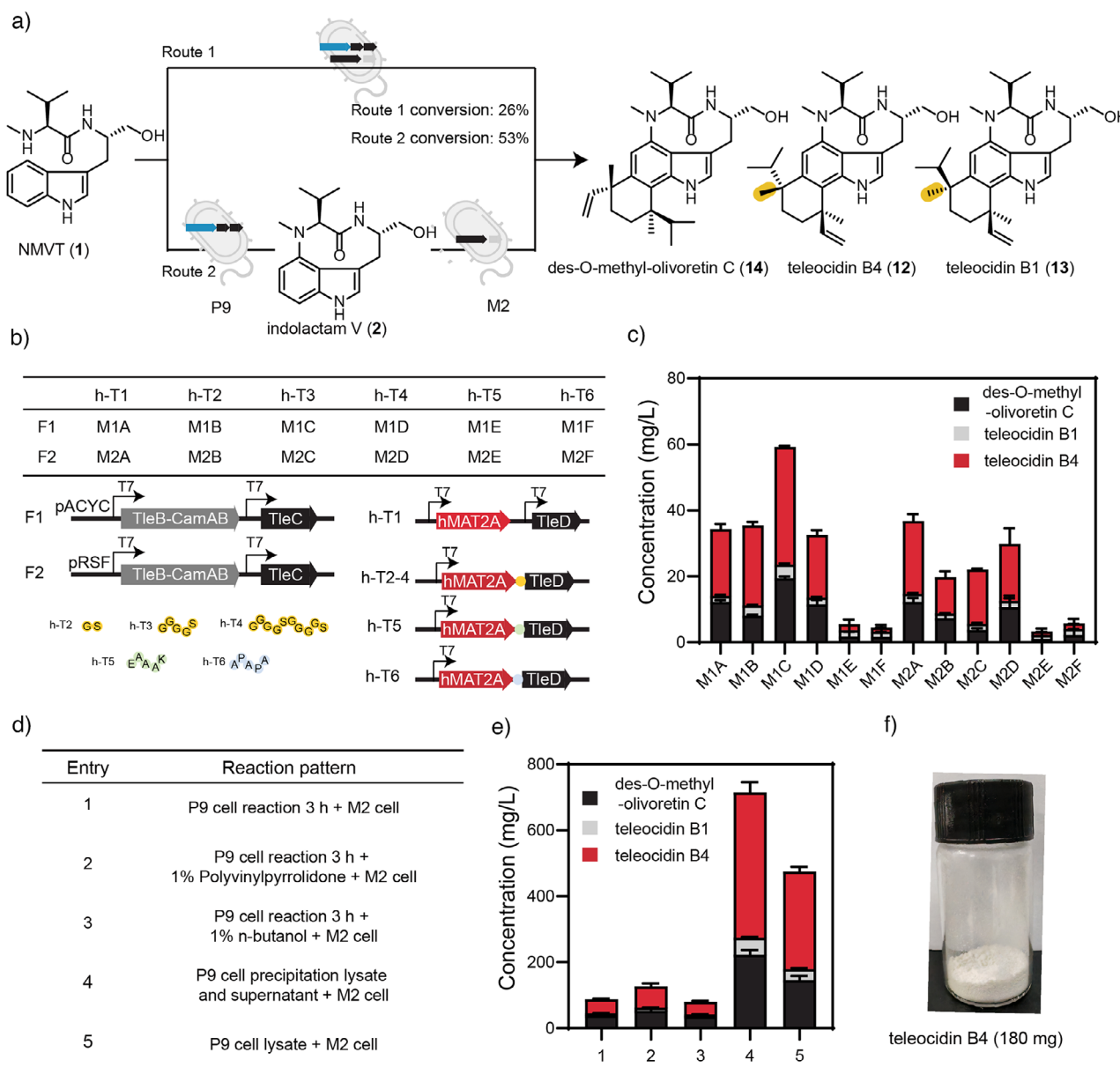


**Figure 4.** Engineering cell platform for conversion of NMVT to teleocidin B. a) Schematic diagram of the teleocidin B production that utilizes NMVT. The system is composed of single or double cells that express all pathway proteins. The bipartite cellular production system expresses TieB-CamAB in P9 cell and TieC, hMAT2A, and TieD in M2 cell. b) Engineered pathway for teleocidin B production in *E. coli*. The system includes two plasmids with antibiotic markers, which together encode for six pathway proteins. pACYC or pRSF series encode for TieB-CamAB and TieC proteins. The pCDF series encodes for hMAT2A and TieD protein or hMAT2A-TieD fusion protein. G: Gly, S: Ser, E: Glu, A: Ala, K: Lys. c) Teleocidin B production titers of 12 engineered strains. Data are of three biological replicates. d) Reaction patterns of continuous production of teleocidin B. 1% PVP40 or 1% *n*-butanol was added to P9 and M2 cell reaction system. P9 cell supernatants and its cell precipitation lysate, or P9 cell lysate, were substrates of M2 cells. e) Teleocidin B production titers of different sequential reaction patterns. Data are of three biological replicates. f) Purified teleocidin B4 product obtained from fermentation.

demonstrating the efficacy of our modular bioprocessing strategy.

To evaluate the scalability of our engineered *E. coli* platform for teleocidin B (**12–14**) biosynthesis from NMVT (**1**), we first propagated M2 catalyst cells via high-density fermentation. The cellular reaction mixture of strain P9 was subsequently lysed, clarified by centrifugation, and the resultant supernatant was subjected to M2-catalyzed biotransformation. This process efficiently converted precursor

intermediates into teleocidin B derivatives, yielding a total of 300 mg of purified compounds (**12–14**), which underscore the system's robust industrial scalability (Figure 4f). Through rational metabolic engineering and pathway optimization, we have established a hybrid chemoenzymatic pipeline. This innovation leverages methyl tryptophan as a cost-effective feedstock, enabling high-titer, scalable synthesis of teleocidin family natural products and structurally related analogs. The modular design of this platform—combining microbial

fermentation with enzymatic catalysis—positions it as a transformative approach for complex monoterpenoid indole alkaloids production at commercial scales.

## Conclusion

In this study, we established a scalable chemoenzymatic platform enabling divergent synthesis of 13 structurally diverse teleocidin B congeners and derivatives, combining modular enzyme engineering with rapid chemical synthesis for efficient large-scale production. Central to this achievement was the rapid, large-scale generation of NMVT substrates via optimized chemical synthesis. Through targeted protein engineering, we enhanced the catalytic activity of key enzymes, establishing a two-strain co-culture system that converts NMVT to teleocidin B with exceptional efficiency, reaching a maximum titer of 714.7 mg L<sup>-1</sup>. By truncating the electron transfer pathway between its [2Fe-2S] cluster and heme cofactor, we significantly improved its catalytic turnover, enabling efficient indolactam V production. This intermediate was subsequently shuttled to a secondary host strain expressing a chimeric hMAT2A-TleD fusion protein, along with TleC, to complete teleocidin B biosynthesis under mild, environmentally benign conditions.

To further demonstrate platform flexibility, we engineered a single-cell factory capable of directly producing structurally complex natural products, including indolactam V, teleocidin A1, pendolmycin, and teleocidin B. This system yielded five novel indolactam V analogs and two teleocidin A1 derivatives not previously observed in nature. Industrial scalability was validated through pilot-scale fermentations, yielding 430 mg indolactam V, 170 mg teleocidin A1, and 300 mg of teleocidin derivatives. Collectively, these results establish a paradigm for de novo biosynthesis of high-value natural products, combining modular chemoenzymatic strategies with scalable microbial chassis. While the TleB variants presented here represent initial structural explorations, the integrated chemoenzymatic platform demonstrates transformative potential for indole alkaloid biosynthesis, particularly through its modular design and scalable operation. This integrated approach not only unlocks access to diverse teleocidin analogs but also provides a blueprint for sustainable, industrial-scale production of complex monoterpenoid indole alkaloids.

## Author Contributions

All authors have read, discussed, and contributed to the manuscript.

## Acknowledgements

The authors thank the National Natural Science Foundation of China (No. 32370045 to H.S.), the Guangdong Basic and Applied Basic Research Foundation (No. 2024A1515011373

to H.S.), and the Shenzhen Science and Technology Program (Grant No. JCYJ20240813111400001).

## Conflict of Interests

The authors declare no conflict of interest.

## Data Availability Statement

The data that support the findings of this study are available from the corresponding author upon reasonable request.

**Keywords:** Chemoenzymatic synthesis • Dual-cell factory • Monoterpenoid indole alkaloids • Protein-engineered P450 system • Teleocidin family

- [1] P. E. Thompson, A. Bayles, B. Olszewski, J. A. Waitz, *Science* **1965**, 148, 1240–1241.
- [2] L. Rubinstein, A. Rein, *Nature* **1974**, 248, 226–228.
- [3] B. Hong, D. Grzech, L. Caputi, P. Sonawane, C. E. R. López, M. O. Kamileen, N. J. Hernández Lozada, V. Grabe, S. E. O'Connor, *Nature* **2022**, 607, 617–622.
- [4] J. Zhang, L. G. Hansen, O. Gudich, K. Viehriq, L. M. M. Lassen, L. Schrübbers, K. B. Adhikari, P. Rubaszka, E. Carrasquer-Alvarez, L. Chen, V. D'Ambrosio, B. Lehka, A. K. Haidar, S. Nallapareddy, K. Giannakou, M. Laloux, D. Arsovska, M. A. K. Jørgensen, L. J. G. Chan, M. Kristensen, H. B. Christensen, S. Sudarsan, E. A. Stander, E. Baidoo, C. J. Petzold, T. Wulff, S. E. O'Connor, V. Courdavault, M. K. Jensen, J. D. Keasling, *Nature* **2022**, 609, 341–347.
- [5] S. A. Bradley, B. J. Lehka, F. G. Hansson, K. B. Adhikari, D. Rago, P. Rubaszka, A. K. Haidar, L. Chen, L. G. Hansen, O. Gudich, K. Giannakou, B. Lengger, R. T. Gill, Y. Nakamura, T. D. de Bernonville, K. Koudounas, D. Romero-Suarez, L. Ding, Y. Qiao, T. M. Frimurer, A. A. Petersen, S. Besseau, S. Kumar, N. Gautron, C. Melin, J. Marc, R. Jeanneau, S. E. O'Connor, V. Courdavault, J. D. Keasling, *Nat. Chem. Biol.* **2023**, 19, 1551–1560.
- [6] H. Fujiki, Y. Tanaka, R. Miyake, U. Kikkawa, Y. Nishizuka, T. Sugimura, *Biochem. Biophys. Res. Commun.* **1984**, 120, 339–343.
- [7] N. F. Fine Nathel, T. K. Shah, S. M. Bronner, N. K. Garg, *Chem. Sci.* **2014**, 5, 2184.
- [8] M. M. H. Fujiki, M. Nakayasu, M. Terada, T. Sugimura, R. E. Moore, *Proc. Natl. Acad. Sci. USA* **1981**, 78, 3872–3876.
- [9] M. S. H. Fujiki, N. Matsukura, T. Sugimura, S. Takayama, *Carcinogenesis* **1982**, 3, 895–898.
- [10] C. E. Antal, A. M. Hudson, E. Kang, C. Zanca, C. Wirth, N. L. Stephenson, E. W. Trotter, L. L. Gallegos, C. J. Miller, F. B. Furnari, T. Hunter, J. Brognard, A. C. Newton, *Cell* **2015**, 160, 489–502.
- [11] M. Takashima, H. Saka, *Bull. Agr. Chem. Soc. Japan* **1960**, 24, 647–651.
- [12] L. Zhang, S. Hoshino, T. Awakawa, T. Wakimoto, I. Abe, *ChemBioChem* **2016**, 17, 1407–1411.
- [13] H. Nakamura, K. Yasui, Y. Kanda, P. S. Baran, *J. Am. Chem. Soc.* **2019**, 141, 1494–1497.
- [14] S. Nakatsuka, T. Masuda, T. Goto, *Tetrahedron Lett.* **1986**, 27, 6245–6248.
- [15] K. G. Brian, D. Dangel, S. W. Youn, B. Sezen, D. Sames, *J. Am. Chem. Soc.* **2002**, 124, 11856–11857.

- [16] D. Tanner, P. Vital, P. O. Norrby, *Synlett*. **2006**, 18, 3140–3144.
- [17] S. Nakatsuka, T. Masuda, T. Goto, *Tetrahedron Lett.* **1987**, 28, 3671–3674.
- [18] H. Muratake, M. Natsume, *Tetrahedron* **1991**, 47, 8535–8544.
- [19] K. Madduri, D. Acharya, A. Lescalette, J. McFadden, P. Ketterer, J. Bing, B. Raman, *ACS Synth. Biol.* **2024**, 13, 3711–3723.
- [20] F. He, T. Mori, I. Morita, H. Nakamura, M. Alblova, S. Hoshino, T. Awakawa, I. Abe, *Nat. Chem. Biol.* **2019**, 15, 1206–1213.
- [21] I. Morita, T. Mori, T. Mitsuhashi, S. Hoshino, Y. Taniguchi, T. Kikuchi, K. Nagae, N. Nasu, M. Fujita, T. Ohwada, I. Abe, *Angew. Chem. Int. Ed.* **2020**, 59, 3988–3993.
- [22] X. Ge, Y. Long, J. Wang, B. Gu, Z. Yang, Y. Feng, S. Zheng, Y. Li, W. Yan, H. Song, *Sci. China Chem.* **2023**, 66, 3232–3241.
- [23] T. Mori, L. Zhang, T. Awakawa, S. Hoshino, M. Okada, H. Morita, I. Abe, *Nat. Commun.* **2016**, 7, 10849.
- [24] T. Awakawa, L. Zhang, T. Wakimoto, S. Hoshino, T. Mori, T. Ito, J. Ishikawa, M. E. Tanner, I. Abe, *J. Am. Chem. Soc.* **2014**, 136, 9910–9913.
- [25] C. Wang, B. Zada, G. Wei, S. W. Kim, *Bioresour. Technol.* **2017**, 241, 430–438.
- [26] S. H. Jeong, J. B. Park, Y. Wang, G. H. Kim, G. Zhang, G. Wei, C. Wang, S. W. Kim, *Metab. Eng.* **2021**, 65, 178–184.
- [27] K. B. Reed, S. M. Brooks, J. Wells, K. J. Blake, M. Zhao, K. Placido, S. d'Oelsnitz, A. Trivedi, S. Gadhiyar, H. S. Alper, *Nat. Commun.* **2024**, 15, 3188.
- [28] H. Zhou, Y. Zhang, C. P. Long, X. Xia, Y. Xue, Y. Ma, M. R. Antoniewicz, Y. Tao, B. Lin, *Nat. Commun.* **2024**, 15, 2372.
- [29] S. Y. Park, H. Eun, M. H. Lee, S. Y. Lee, *Nat. Catal.* **2022**, 5, 726–737.
- [30] D. Yang, S. Y. Park, S. Y. Lee, *Adv. Sci.* **2021**, 8, 2100743.
- [31] L. Guo, W. Diao, C. Gao, G. Hu, Q. Ding, C. Ye, X. Chen, J. Liu, L. Liu, *Nat. Catal.* **2020**, 3, 307–318.
- [32] Y. Long, S. Zheng, Y. Feng, Z. Yang, X. Xu, H. Song, *ACS Catal.* **2022**, 12, 9857–9863.
- [33] S. Y. Li, L. M. Podust, D. H. Sherman, *J. Am. Chem. Soc.* **2007**, 129, 12940–12941.
- [34] N. Fujita, F. Sumisa, K. Shindo, H. Kabumoto, A. Arisawa, H. Ikenaga, N. Misawa, *Biosci. Biotechnol. Biochem.* **2009**, 73, 1825–1830.
- [35] A. Robin, G. A. Roberts, J. Kisch, F. Sabbadin, G. Grogan, N. Bruce, N. J. Turner, S. L. Flitsch, *Chem. Commun.* **2009**, 14, 2478–2480.
- [36] Y. W. C. Sun, B. Hu, J. Wang, J. Zhou, J. Li, J. Chen, G. Du, B. J. Wang, X. R. Zhao, *Angew. Chem. Int. Ed.* **2025**, 5, e202423209.
- [37] X. Zhang, Y. Hu, W. Peng, C. Gao, Q. Xing, B. Wang, A. Li, *Front. Chem.* **2021**, 9, 649000.
- [38] Z. Wang, S. Shaik, B. Wang, *J. Am. Chem. Soc.* **2021**, 143, 1005–1016.
- [39] G. A. Roberts, A. Çelik, D. J. B. Hunter, T. W. B. Ost, J. H. White, S. K. Chapman, N. J. Turner, S. L. Flitsch, *J. Biol. Chem.* **2003**, 278, 48914–48920.
- [40] A. W. Munro, D. G. Leys, K. J. McLean, K. R. Marshall, T. W. B. Ost, S. Daff, C. S. Miles, S. K. Chapman, D. A. Lysek, C. C. Moser, C. C. Page, P. L. Dutton, *Trends Biochem. Sci.* **2002**, 27, 250–257.
- [41] L. Zhang, Z. Xie, Z. Liu, S. Zhou, L. Ma, W. Liu, J. W. Huang, T. P. Ko, X. Li, Y. Hu, J. Min, X. Yu, R. T. Guo, C. C. Chen, *Nat. Commun.* **2020**, 11, 2676.
- [42] H. Gao, Y. Fan, X. He, X. Peng, Z. Li, Y. Zheng, S. Ji, L. Ye, A. Li, B. Wang, J. Zhao, *ACS Catal.* **2024**, 14, 10658–10669.
- [43] S. Singh, J. Zhang, T. D. Huber, M. Sunkara, K. Hurley, R. D. Goff, G. Wang, W. Zhang, C. Liu, J. Rohr, S. G. Van Lanen, A. J. Morris, J. S. Thorson, *Angew. Chem. Int. Ed.* **2014**, 53, 3965–3969.
- [44] F. Yu, M. Li, C. Xu, B. Sun, H. Zhou, Z. Wang, Q. Xu, M. Xie, G. Zuo, P. Huang, H. Guo, Q. Wang, J. He, *Biochem. J.* **2016**, 473, 4385–4397.

Manuscript received: April 24, 2025

Revised manuscript received: June 25, 2025

Accepted manuscript online: July 14, 2025

Version of record online: ■■■■■